MARITIME TRANSPORTATION RESEARCH AND EDUCATION CENTER
TIER 1 UNIVERSITY TRANSPORTATION CENTER
U.S. DEPARTMENT OF TRANSPORTATION

Informing Post-Disaster Restoration through Modeling Interdependent Agriculture and Transportation Networks

August 13, 2018 - October 31, 2021

PI: Sarah G. Nurre Pinkley, Ph.D.
Co-PI: Kelly M. Sullivan, Ph.D.
Co-PI: Benjamin R. K. Runkle, Ph.D., P.E.
Hieu T. Bui
Jakhongir Khatamov
University of Arkansas

Janey Camp, Ph.D.
Katherine Turner
Nicholas Laning
Vanderbilt University

December 2021

FINAL RESEARCH REPORT
Prepared for:
Maritime Transportation Research and Education Center

University of Arkansas
4190 Bell Engineering Center
Fayetteville, AR 72701
479-575-6021

ACKNOWLEDGEMENT

This material is based upon work supported by the U.S. Department of Transportation under Grant Award Number 69A3551747130. The work was conducted through the Maritime Transportation Research and Education Center at the University of Arkansas.

This research is supported by the Arkansas High Performance Computing Center which is funded through multiple National Science Foundation grants and the Arkansas Economic Development Commission.

DISCLAIMER

Contents

List of Figures

List of Tables

1 Project Description

In the United States, Arkansas is well suited for the study of the dependence of the food and agriculture sector (FA) on the transportation sector: the FA sector plays a relatively important role in the state's economy. In 2019 this sector contributed nearly 10% of Arkansas' GDP, including 1.5% and 5.9% from agricultural production and processing respectively [English et al., 2020]. This share of the state's economy is 2.6 times greater than for the U.S. as a whole. In 2019, the state was ranked first nationally in rice production, second in broiler chickens, third in catfish, and fifth in turkeys [USDA-NASS]. Maintaining high crop and animal production levels depends on parts of many other sectors within the economy, including power plants, chemical manufacturing, water supplies and distribution, transportation networks, and agricultural production facilities [Ahumada and Villalobos, 2009]. In Arkansas, there are industries involved in the most common stages of the agricultural supply chain [English et al., 2020], including production, processing/packaging, distribution, retailing, and consumption & disposal [Kinsey, 2001].

Agricultural supply chains are inherently complex due to their interdependency with critical infrastructure systems including energy, water, and maritime and multimodal transportation. This complexity is increased due to the dependence on time-sensitive and capital-intensive operations, uncertain natural events, and volatile commodity markets as well as their position within rural and low socioeconomic communities. When functioning, the U.S. transportation network provides a backbone that enables the transport of agricultural inputs (e.g., chemicals, seeds) and outputs (e.g., raw/processed goods).

However, disruptions to transportation mode(s) cause severe and cascading operational and economic damage, which are magnified due to the inherent complexity of agriculture supply chains. For example, Hurricane Harvey's impact on ports and rail was detrimental to agriculture because it occurred during harvest and caused impassable roads through the region [Wiener et al., 2020]. Delays on inland waterways impacted the timely delivery of necessary fertilizers. An example from the global COVID-19 crisis is that while the crisis reduced transportation demand, the shift in container traffic created a loss of empty containers for shipments [Gray, 2020]. On a local scale, the food and agriculture sector often relies on transport between farms, chemical supply companies, and mills or processing facilities, all within a close radius ($\sim$ 25 km), and depends on a robust truck transportation infrastructure (a finding from ERISF project and Doerpinghaus et al. [2021] in preparation, 2021). The May, 2021, Memphis bridge closure affected agricultural supply chains through both reduced barge traffic and slower truck traffic [Hightower, 2021]. Weather can destroy road links in agricultural regions while also reducing the productive capacity of those regions [Smith et al., 2019]. Weather and many other issues can cause unplanned lock outages and other disruptions to the maritime transport system; as these disruptions affect supply chain commodities that are shipped in bulk, the agriculture sector is impacted at an outsized rate to its share of the economy [MARAD, 2017].

Prior research fails to capture how these important details—including different transportation modes, sensitivity to time and decentralized geographic space, and the economic impacts for rural communities—impact how transportation should be used when a disruption has occurred and how to coordinate restoration activities across interdependent infrastructure systems. We address this research gap by modeling the operation and restoration of an

interdependent set of transportation and agriculture networks. We present a mixed integer linear programming formulation which seeks to maximize the expected yield for a set of rice farms throughout the state of Arkansas under scenarios where the amount and timeliness of fertilizer delivery are affected by a disrupted transportation network. We validate the model using real data for a case study in Arkansas. This dataset includes the location and acreage of rice farms in Arkansas, fertilizer demand, and a multimodal transportation network comprised of road, rail, and waterway networks. For this dataset, we created disruption scenarios for different transportation modes with different severity, location, and duration. Using these data, we ran extensive computational experiments to deduce operational and restoration insights on the interdependence and resiliency of transportation and agriculture systems.

We note that this work is performed by an interdisciplinary, multi-institution team that was developed to provide multiple perspectives on the systemic challenges presented by transportation disruptions to the agricultural sector. The interdisciplinary approach has been encouraged for co-developing flexible modeling platforms and scenario-based analysis with a specific user community in mind [Jarke et al., 1998]. The authors thus bring their expertise in restoration planning [Nurre et al., 2012], interdependent network modeling [Enayaty Ahangar et al., 2020], agricultural sustainability [Carroll et al., 2020], and Python programming (Hieu) from the University of Arkansas MarTREC consortium. Complementing this work from Vanderbilt University, Dr. Camp brings expertise in natural and man-made systems utilizing geospatial technologies [Nelson et al., 2015]. This collaborative approach aims to construct a realistic agricultural delivery disruption scenario within a novel, state-of-the-science modeling framework.

This report proceeds as follows. In Section 2, we provide an overview of literature related to the interdependencies between FA and transportation. In Section 3, we formally define the methodological approach including the problem statement, notation, and our mixed integer programming formulation. In Section 4, we present the transportation and FA data used for our Arkansas case study. In Sections 5 and 6, we outline our computational experiments and findings. Lastly, in Sections 7 and 8, we conclude and present avenues for future work.

2 Literature Review

Interdependencies between FA and other sectors of the economy have received significant attention in the literature. Building upon the input-output model of Leontief [1951, 1966], researchers have characterized the economic relationships of FA with other industries [Heady and Schnittker, 1957, Schnittker, 1956, Karkacier and Goktolga, 2005] and infrastructure sectors [Zimmerman et al., 2016]. The Leontief input-output model has been extended to model infrastructure interdependencies for the purpose of assessing risks due to natural or man-made disasters, which may reduce the functionality of multiple infrastructures [Haimes and Jiang, 2001, Haimes et al., 2005]. These models characterize interdependence at the sectoral level, not at the individual component level. As a result, these models are neither ideal for characterizing the operational impact of a specific disruption scenario (e.g., identifying which specific entities in an agricultural supply chain would be most affected by disruption of specific nodes or links in another infrastructure network) nor helpful for prioritizing recovery

efforts in response to such a scenario (e.g., which failed links should be repaired first).

Over the last two decades, component-level infrastructure interdependencies have been studied in greater detail, beginning with the work of Rinaldi et al. [2001] who provided a framework for classifying operational interdependencies. Many operational interdependencies related to the "lifeline" sectors—transportation, water, energy, and communications—have been described in the literature (see [Ouyang, 2014, Mendonça and Wallace, 2006] for example). Related to the FA sector, there are only a few recent studies [Zimmerman et al., 2016, Doerpinghaus et al., 2021] that characterize operational interdependencies with other infrastructure sectors. Separate from the infrastructure interdependency literature, other research communities have identified interactions among food security, water security, and energy security—described as the "water-energy-food nexus"—with the aim of more sustainably managing these critical resources [Scott et al., 2015, D'Odorico et al., 2018]. Whereas much of the component-level FA interdependence research is qualitative in nature, our work quantitatively models the dependence of FA on multimodal transportation.

This research related to the FA sector and other infrastructure sectors fall under a large body of research which broadly examines the resilience of interdependent infrastructures. A review on the resilience of interdependent infrastructures [Ouyang, 2014] demonstrates empirical (McDaniels, et al. 2007), economic theory [Haimes et al., 2005], and network-based (Lee, Mitchell and Wallace 2007, Cavdaroglu, et al. 2013) approaches to improve resilience. Commonly, the Rinaldi classification of interdependence Rinaldi et al. [2001] is used to capture how systems interact, however recent interdependency classifications are emerging with a focus on restoration (Chang, McDaniels and Mikawoz, et al. 2007, Sharkey, et al. 2016). A subset of this work focuses on resilience of multimodal transportation. For example, He et al. 2021 perform a node criticality analysis by examining how the removal of a single node impacts the total travel time within a multimodal transportation network. Research has previously considered disruptions to multimodal transportation systems from a number of perspectives, including economic analysis of inland waterway disruptions considering shippers' option to transfer cargo to alternative modes [Güler et al., 2012, Oztanriseven and Nachtmann, 2017] and simulation of multimodal commodity movements in the presence of disruption [Burgholzer et al., 2013, Azucena et al., 2021].

To fundamentally capture the disruptions to multimodal transportation, we review how to model the operations of multimodal transportation systems. SteadieSeifi et al. [2014] survey the application of operations research techniques to multimodal transportation planning problems. The authors classify the existing literature into strategic, tactical planning, and operational planning with dynamicity and stochasticity problems. Our work falls under the class of tactical planning problems using a static service network design modeling approach. Within this broad class of problems, most researchers use network flow to represent the movement of transporting entities or commodities and seek to minimize costs (e.g., Anghinolfi et al. 2011, Caris et al. 2012, Crainic et al. 2006), minimize (waiting) time (e.g., Ayar and Yaman 2012, Cho et al. 2012, Pazour et al. 2010), or maximize profit (e.g., Gelareh and Pisinger 2011, Shintani et al. 2007). Our research is unique in its consideration of how the amount of fertilizer demand satisfied impacts the expected yield months later.

Researchers have examined the restoration of a broad set of interdependent infrastructures including multimodal transportation systems. While we continue by focusing on the restoration of multimodal transportation networks, we first point the reader to a recent re-

view on the restoration of a broad set of interdependent infrastructures using network flow (Sharkey et al. 2021). Chen and Miller-Hooks [2012] present a stochastic mixed-integer program to select an optimal set of arcs to restore immediately following a disruption to an intermodal freight network. They seek to maximize the expected fraction of demand met for a set of origin-destination pairs subject to level-of-service constraints which incorporate the timeliness of satisfying demand. Similarly, Miller-Hooks et al. [2012] present a two-stage stochastic program for an intermodal freight network which first selects preparedness actions and second, after the realization of a disruption scenario, selects restoration actions. All actions are subject to a shared budget constraint. Huang et al. [2011] capture restoration in a different context as they forecast the duration of the disruption to determine when and where shipments should be rerouted.

3 Methodological Approach

This study applied a network-based optimization model to describe interdependent relationships between the agriculture sector and the transportation sector. The infrastructure systems consist of a collection of nodes and arcs through which commodities (fertilizer in this research) flow from the supply nodes to the demand nodes. In addition, there are transshipment nodes that serve as intermediate points and have neither supply nor demand, and intermodal nodes which are a subset of transshipment nodes. Intermodal nodes are used to enable the flows to switch from one transporting mode to another, and they also enable storing inventory for later use. Each node has its own capacity that defines the maximum number of mode-specific transporting entities that can wait at the node. Each arc has an associated traversal time and a capacity that limits the number of transporting entities and the number of containers moved on the arc per unit time. The transportation network comprises three transporting modes: road, rail, and water. Trucks, trains, and barges are used as the transporting entities for each mode, respectively. The model consists of a discrete number of time periods, which enables modeling the flow of commodities over time.

Interactions between the agriculture sector and the transportation system are modeled at the demand nodes, which represent agricultural production sites that require as input the commodity that is being transported through the network. Specifically, our model rewards demand satisfied through the transportation network as a means of quantifying the agricultural yield by receiving the commodity input by a given time. The infrastructure systems are subject to disruptions such as floods, ice storms, and droughts that degrade the services of the transportation network, resulting in reduced agricultural production. To mitigate the impacts of disruptions, we need to identify the set of damaged arcs to repair to restore the transportation network services. Due to a limited budget, the entire network cannot be repaired at once, therefore, only those components that maximize the expected total rice yield would be repaired. It should be noted that there are some arcs whose operationality cannot be restored at all after a disruption. Thus, the available budget will not be considered for those arcs.

3.1 Assumptions

We made several assumptions to reduce the complexity of the model: (1) The transporting entities (e.g., trucks, trains, barges) for each mode are identical. They have the same container capacity, and they are moving at constant speeds (i.e., 70 mph for trucks, 20 mph for trains, and 6 mph for barges). (2) The capacity for loading and unloading at intermodal nodes is independent of mode. (3) The sets of arcs for any two modes are disjoint. The intermodal nodes are used to switch the flow of commodities from one mode to another in the network. (4) We do not explicitly model the cost and time associated with passing through intermodal nodes. (5) We do not model the movement of empty containers or empty transporting entities in the model. (6) Each time period in the model is equivalent to thirty minutes. Therefore, we assume that the minimum traversal time for each arc is thirty minutes. This assumption was made to help us to better represent the network in the urban area where there are many short arcs. (7) The quantity of supply matches the sum of all required demands among the counties. (8) We represent the amount of demand and supply in terms of containers.

3.2 Notation

Sets:

Name	Description
N	set of nodes
N'	set of intermodal nodes
F	set of demand nodes
H	set of supply nodes
M	set of transportation modes
A	set of arcs
A'	set of unrestorable arcs after a disruption
K	set of commodities
N^m	collection of nodes for each mode
A^m	collection of arcs for each mode
T	time periods

Parameters:

Name	Description
f_i^k	demand of commodity k at demand node i
h_i^k	supply of commodity k at demand node i
d_{ij}	traversal distance of arc (i, j)
τ_{ij}	traversal time of arc (i, j)
u_{ij}	container capacity of arc (i, j)
$\overline{u}_{ij}$	transporting entities capacity of arc (i, j)
u_{ijt}^m	maximum number of containers per transporting entity on arc (i, j) at time t
λ_{ij}	level of functionality of arc (i, j)
μ_i	waiting container capacity at node i
q_i	inventory capacity of intermodal node i
ϕ_i	loading/unloading capacity of intermodal node i
ν_t^m	maximum number of transporting entities of mode m at time t
p^m	penalty per unit distance of using entities of mode m
Υ_t	additional yield at time t

Variables:

Name	Description
x_{ijt}^{mk}	# of containers of commodity k move from i to j via mode m at time t
y_{ijt}^m	# of transporting vehicles of mode m move from i to j at time t
w_{it}^{mk}	# of waiting containers of commodity k at node i at time t
$w_{it}^{\phi k}$	# of containers of commodity k in inventory at node i at time t
v_{it}^m	# of transporting entities of mode m waiting at node i at time t
χ_{it}^{mk}	# of loaded containers of commodity k at intermodal node i at time t
η_{it}^{mk}	# of unloaded containers of commodity k at intermodal node i at time t
z_{it}^k	amount of commodity k demand satisfied at demand node i at time t
α_{it}^k	amount of commodity k supply used at node i at time t
δ_{ijt}	cumulative percentage of operational status that has been restored for arc (i, j) at time t
D_{ijt}	positive change in cumulative restoration of arc (i, j) at time t

3.3 Mathematical Model

$$\max \quad \sum_{i\in F}\sum_{k\in K}\sum_{t\in T} z_{it}^{k}\Upsilon_{t} - \sum_{(i,j)\in A^{m}}\sum_{m\in M}\sum_{k\in K}\sum_{t\in T} x_{ijt}^{mk} d_{ij} p^{m}$$

s.t.

$$w_{it-1}^{mk} + \sum_{(j,i)\in A^{m}} x_{jit-\tau_{ij}}^{mk} - w_{it}^{mk} + \sum_{(i,j)\in A^{m}} y_{ijt}^{mk} = 0, \quad \begin{array}{l}\forall m \in M, \forall k \in K \\ \forall i \in N \setminus \{N', F, H\}\end{array} \tag{1}$$

$$w_{it-1}^{mk} + \chi_{it}^{mk} + \sum_{(j,i)\in A^{m}} x_{jit-\tau_{ij}}^{mk} - w_{it}^{mk} + \eta_{it}^{mk} + \sum_{(i,j)\in A^{m}} x_{ijt}^{mk} = 0, \quad \forall m \in M, \forall i \in N', \forall k \in K \tag{2}$$

$$\sum_{(j,i)\in A^{m}} x_{jit-\tau_{ij}}^{mk} - \sum_{(i,j)\in A^{m}} x_{ijt}^{mk} - z_{it}^{k} = 0, \quad \forall m \in M, \forall i \in F, \forall k \in K \tag{3}$$

$$\sum_{(j,i)\in A^{m}} x_{jit-\tau_{ij}}^{mk} - \sum_{(i,j)\in A^{m}} x_{ijt}^{mk} + \alpha_{it}^{k} = 0, \quad \forall m \in M, \forall i \in H, \forall k \in K \tag{4}$$

$$\sum_{t\in T} z_{it}^{k} - f_{i}^{k} \leq 0, \quad \forall i \in F, \forall k \in K \tag{5}$$

$$\sum_{t\in T} \alpha_{it}^{k} - h_{i}^{k} \leq 0, \quad \forall i \in H, \forall k \in K \tag{6}$$

$$\left(w_{it}^{\phi k} - w_{it-1}^{\phi k}\right) - \left(\sum_{m\in M} \eta_{it}^{mk} - \sum_{m\in M} \chi_{it}^{mk}\right) = 0, \quad \forall i \in N', \forall k \in K, \forall t \in T \tag{7}$$

$$\sum_{m\in M}\sum_{k\in K} (\chi_{it}^{mk} + \eta_{it}^{mk}) - \phi_{i} \leq 0, \quad \forall i \in N', \forall t \in T \tag{8}$$

$$\sum_{k\in K} w_{it}^{\phi k} - q_{i} \leq 0, \quad \forall i \in N', \forall t \in T \tag{9}$$

$$\sum_{k\in K} w_{it}^{mk} - \mu_{i} \leq 0, \quad \forall m \in M, \forall i \in N, \forall t \in T \tag{10}$$

$$\sum_{k\in K} w_{it}^{mk} - u_{it}^{m} v_{it}^{m} \leq 0, \quad \forall m \in M, \forall i \in N, \forall t \in T \tag{11}$$

$$\sum_{k\in K} x_{ijt}^{mk} - u_{ijt}^{m} y_{ijt}^{m} \le 0, \quad \begin{array}{l}\forall m \in M, \forall (i,j) \in A^m, \\ \forall t \in T\end{array} \tag{12}$$

$$\sum_{(i,j)\in A^m} \sum_{t'=t-\tau_{ij}+1}^{t} y_{ijt'}^{m} + \sum_{i\in N^m} (v_{it}^{m} - v_{it-1}^{m}) - \nu_{t}^{m} = 0, \quad \forall m \in M, \forall t \in T \tag{13}$$

$$\sum_{k\in K} x_{ijt}^{mk} - u_{ij}(\lambda_{ij}^{t'} + \delta_{ij}^{t'}) \le 0, \quad \begin{array}{l}\forall m \in M, \forall (i,j) \in A^m, \\ \forall t = 0, \cdots, |T| - \tau_{ij} + 1, \\ \forall t' = t, t+1, \cdots, t+\tau_{ij} - 1\end{array} \tag{14}$$

$$y_{ijt}^{m} - \overline{u}_{ij}(\lambda_{ij}^{t'} + \delta_{ij}^{t'}) \le 0, \quad \begin{array}{l}\forall m \in M, \forall (i,j) \in A^m, \\ \forall t = 0, \cdots, |T| - \tau_{ij} + 1, \\ \forall t' = t, t+1, \cdots, t+\tau_{ij} - 1\end{array} \tag{15}$$

$$\sum_{(i,j)\in A^m} D_{ijt} - B_t \le 0, \quad \forall t \in T \tag{16}$$

$$\lambda_{ijt} + \delta_{ijt} \le 1, \quad \forall (i,j) \in A^m \setminus A', \forall t \in T \tag{17}$$

$$\delta_{ijt+1} - \delta_{ijt} - D_{ijt+1} \le 0, \quad \forall (i,j) \in A^m, \forall t \in T \setminus \{|T|\} \tag{18}$$

$$y_{ijt}^{m} \ge 0, \text{ integer}, \quad \forall m \in M, \forall (i,j) \in A^m, \forall t \in T \tag{19}$$

$$v_{it}^{m} \ge 0, \text{ integer}, \quad \forall m \in M, \forall i \in N, \forall t \in T \tag{20}$$

$$x_{ijt}^{m} \ge 0, \quad \begin{array}{l}\forall k \in K, \forall m \in M, \\ \forall (i,j) \in A^m, \forall t \in T\end{array} \tag{21}$$

$$w_{it}^{mk} \ge 0, \quad \begin{array}{l}\forall k \in K, \forall m \in M, \\ \forall i \in N, \forall t \in T\end{array} \tag{22}$$

$$x_{it}^{mk} \ge 0, \quad \forall k \in K, \forall i \in N', \forall t \in T \tag{23}$$

$$\chi_{it}^{mk} \ge 0, \quad \begin{array}{l}\forall k \in K, \forall m \in M, \\ \forall i \in N', \forall t \in T\end{array} \tag{24}$$

$$\eta_{it}^{mk} \geq 0, \quad \begin{matrix} \forall k \in K, \forall m \in M, \\ \forall i \in N', \forall t \in T \end{matrix} \tag{25}$$

$$0 \leq \delta_{ijt} \leq 1, \quad \forall (i,j) \in A, \forall t \in T \tag{26}$$

$$0 \leq D_{ijt} \leq 1, \quad \forall (i,j) \in A, \forall t \in T \tag{27}$$

3.4 Description of Model

- The objective function maximizes the total amount of rice yield over the planning horizon minus the cost/penalty for using different transportation modes.
- Constraints (1)–(4) are network flow constraints for non-intermodal, intermodal, demand, and supply nodes, respectively,
- Constraints (5)–(6) limit the demand satisfied and available supply at demand and supply nodes, respectively,
- Constraint (7) is an inventory balance constraint for intermodal nodes,
- Constraint (8) ensures the loading and unloading activities do not exceed the existing capacity at intermodal nodes,
- Constraints (9)–(11) restrict the number of waiting containers and transporting entities at nodes,
- Constraint (12) ensures that the flow on arcs with respect to the number of containers does not exceed the capacity of transporting entities,
- Constraint (13) guarantees that the number of transporting entities does not exceed the maximum available to use for each mode by time,
- Constraints (14)–(15) ensure that the flow on arcs with respect to the number of containers and the number of transporting entities does not exceed the established capacities, respectively,
- Constraint (16) ensures restoration expenses do not exceed the available budget,
- Constraint (17) ensures that the sum of the operational status and restored proportion of an arc are at most 100 percent,
- Constraint (18) ensures that we capture only the positive changes in the operational status of arcs that may occur when the restoration is, indeed, made,
- Constraints (19)–(27) describe the nature of decision variables.

4 Arkansas Data and Case Study

In this section, we present the data used for our case study examining the fertilizer delivery from New Orleans to rice farms in Arkansas. We collected the data from a variety of sources and aggregated the elements to create an interdependent multimodal transportation network with agricultural demand nodes. We disrupt the multimodal transportation network using disruptions scenarios based on historical flood events. We proceed by describing the multimodal transportation network, agricultural demand calculation, and disruptions scenarios.

4.1 Multimodal Transportation Network

The data for road, rail and waterway networks, and the data for intermodal nodes were obtained from the TIGER/Line Shapefiles [U.S. Census Bureau] and were analyzed using ArcGIS software and Python. We first extracted the roads for Arkansas to create the road network, which includes 9,324 arcs and 7,684 nodes. We only kept the roads with the US and interstate types (i.e., I and U code in the RTTYP format according to the Census Bureau code lists) to capture the roads most likely to be used for transportation of fertilizer which also results in a simplified network. We also modified this network to include additional last-mile transportation arcs to connect this network to demand nodes. We explain these modifications when discussing the demand nodes.

We then extracted the major roads in the surrounding states (i.e., Louisiana, Mississippi, Tennessee) that connect the supply node (i.e., New Orleans) to road nodes in Arkansas. By doing so, we can send commodities to the demand nodes through different transporting modes, so they do not rely solely on the waterways. After removing parallel arcs and consolidating chains of degree-two nodes, the road network is comprised of 660 arcs and 114 nodes. Figure 1a represents the consolidated and simplified road network. Note that trucks are still able to travel to the major cities and places that are of interest in this research. Each road node was assigned a unique identification number starting at 0 and ending at 9000.

Similar to the road network, we extracted railways from the Shapefiles. However, the observed data revealed that it consisted of a high number of arcs and nodes that represent abandoned rail yards and segments. Because these arcs and nodes are not currently being used, we removed them from our dataset. In addition, we grouped the arcs and nodes that belong to the railyards together to reduce the complexity of the network. The visual observation of the simplified network showed that there were a few disjoint components that were either eradicated or linked to the rest of the rail network after providing reasonable justifications. As a result, the number of arcs and nodes amounted to 620 and 179, respectively (Fig. 1b). The labels from 30001 to 35000 were assigned to rail nodes.

The navigable waterway network comprises three components: the Red River, the Ouachita River, and the Mississippi River. Because the Arkansas River goes across the state, we divided the straight segment to join at the various locks and dams in between. This step allowed us to create disruption scenarios based on the historical operational data of these locks. To simplify the water network that is outside Arkansas, we combined the arcs and intersected them at the supply node in New Orleans. Therefore, we have three routes to move commodities out of the supply node to the water nodes in Arkansas. In the final water

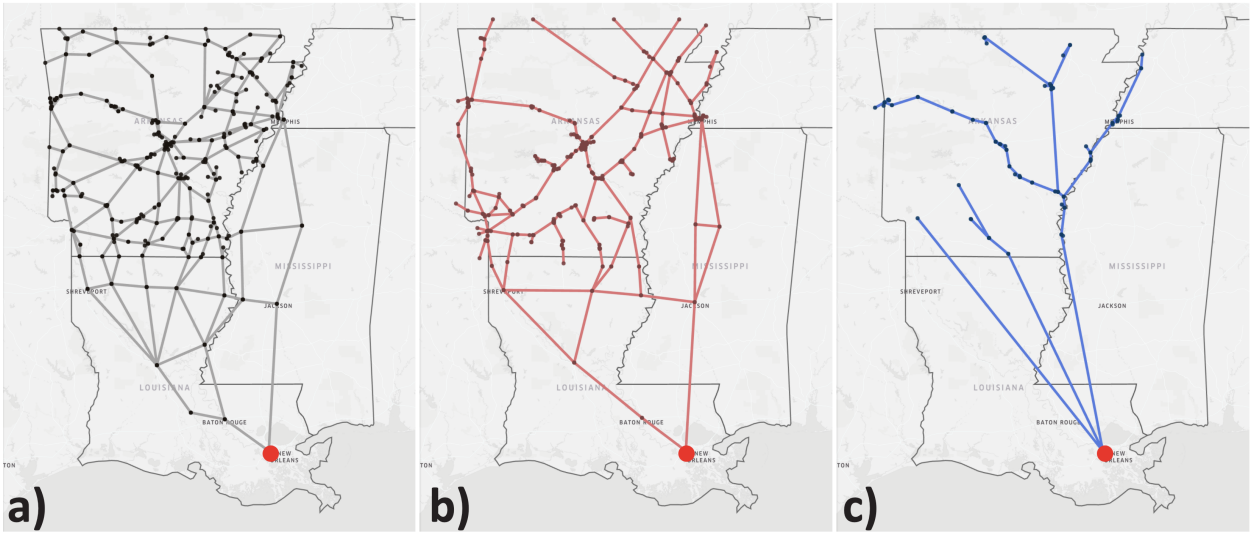

Figure 1: **a)** road, **b)** rail, and **c)** water networks. The red marker denotes the supply node in the network.

network (Fig. 1c), there were 128 arcs and 36 nodes. The labels for water nodes ranged from 40000 to 45000.

In this research, we considered a single supply node only; future researchers can add more supply nodes and connect them to the existing network. We chose a location near New Orleans as the supply node since many nitrogen fertilizer production sites and distribution centers are located around it [The Fertilizer Institute, 2021]. Fig. 1 shows that the supply node (red maker) is connected to the road, rail, and water networks. The supply node was labeled as 80000 and was set with sufficient supply of fertilizer to satisfy all demand. We considered 37 demand nodes in the network (Fig. 2) that were provided by the research team from Vanderbilt University. Each demand node consists of the total acreage, the number of rice elevators, and its geocoordinate. We connected each demand node to its closest road node. This means that the demand nodes can only be accessible by trucks. Each demand node was assigned a unique identification number that starts at 90000.

Vanderbilt University's research team also provided the intermodal node locations. The original data for intermodal nodes consisted of 496 nodes. By creating a visualization of these nodes, we observed that many intermodal nodes appeared redundant. For example, intermodal nodes of similar types (e.g., from the rail to the road modes) are located close to each other. We selected a reasonable subset of the intermodal nodes by calculating the distance from each intermodal node to the mode-specific node. The intermodal node was retained if it was within seven miles from at least two mode-specific nodes. Otherwise, it was removed. As a result, 123 intermodal nodes met this criterion and were included in the transportation network. For these nodes, we assigned numbers ranging from 70000 to 75000.

Based on realistic accounts, we know that fertilizer is predominantly shipped on the waterways, then rail, then roads in an undisrupted environment. However, during the initial testing of the optimization model, we observed that all three transporting modes were used to transport the containers from the supply node. In addition, the water mode was the least preferred mode of all, because the barges have the slowest transit time. For example,

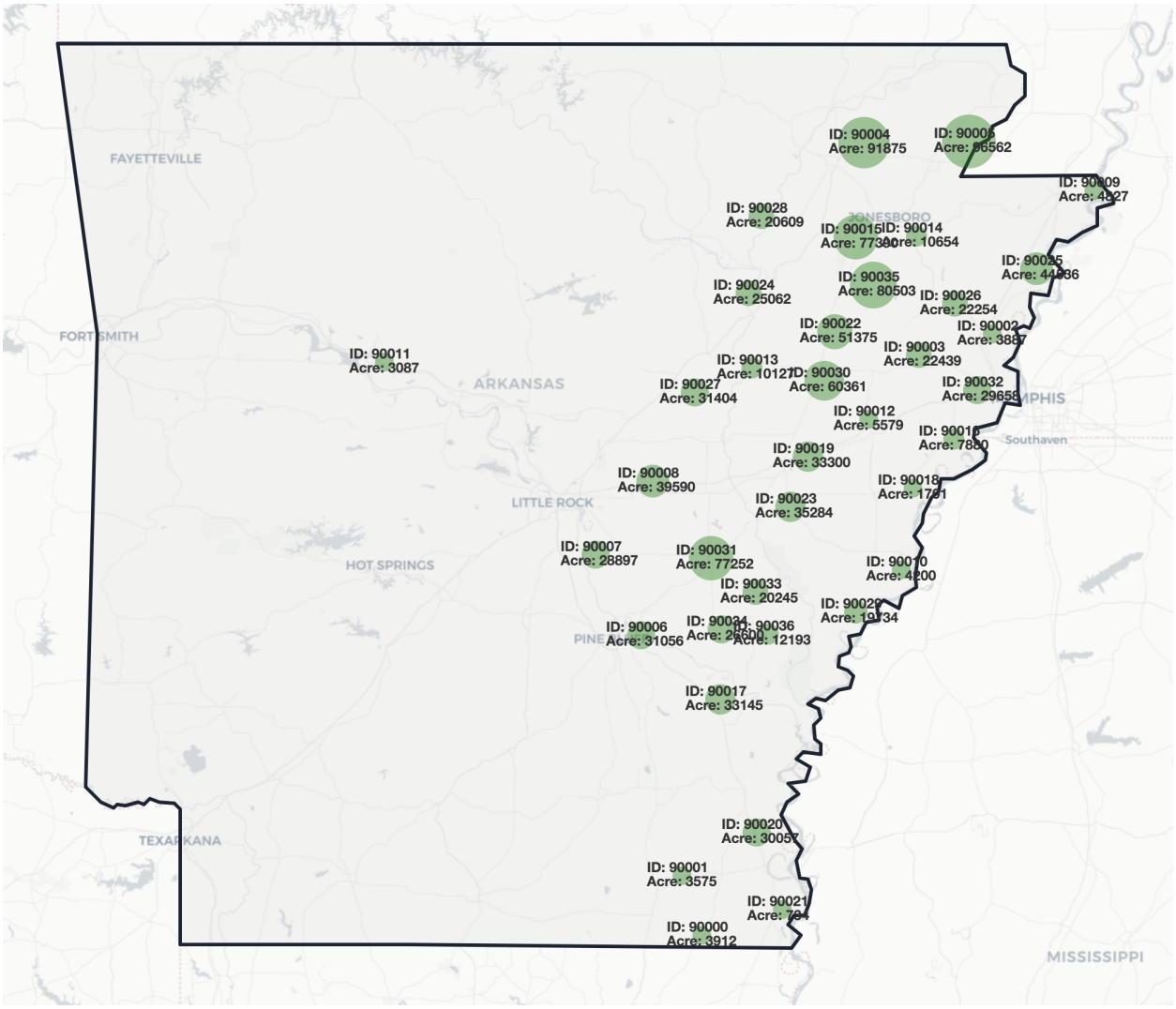

Figure 2: Demand nodes with the node identification number (top), and the total acreage (bottom). The size of the marker represents the relative acreage.

trains could make multiple trips and carry the same number of containers at the same time that barges make one trip. To reflect the realistic nature of the transportation network , we introduced a penalty per unit distance for each transporting mode. In particular, water was prioritized to become the highest means of transportation, next was rail, and last was road. Thus, the values for the penalty terms (i.e., the parameter p^m) were 7, 5, 1 for road, rail, and water, respectively.

4.2 Transportation Network Parameters

In this section, we describe the input parameters necessary for the model. These include the data used for the network including traversal time, capacities for transporting entities and containers traversing the network, waiting, held in inventory, or being loaded/unloaded.

The traversal time is an essential component of the optimization model. The traversal time τ_{ij} for each arc (i, j) was calculated by dividing the great-circle distance between two nodes by the traversal speed (i.e., 70 mph for trucks, 20 mph for trains, and 6 mph for barges). Because the time period in the model is an integer, the traversal time was rounded up to the nearest number of time periods. We initially defined one time period to be equal to 1 hour and assigned zero traversal time for the road, rail, and water arcs that are less than 11, 8, and 4 miles, respectively, as these arcs are very short and do not make a significant impact on the result.

After analyzing the traversal time for road and rail networks, we observed that the majority of the short segments were concentrated around the urban areas or major distribution hubs. By observing the distribution of the traversal time for road and rail networks (Fig. 3), we can see that setting the time period as 1 hour would result in 142 and 310 arcs with the traversal time of 1 hour for rail and road, respectively. However, we can see that the median traversal time for the aforementioned arcs is closer to ½ hour than 1 hour (Fig. 3); therefore, we adjusted the time period to equal ½ hour. We also removed the zero traversal time assumption above as this assumption created 802 arcs (i.e., the total number of arcs is 1,408) with zero traversal time. Although these adjustments increased the computational time of the model (i.e., double the number of periods for optimizing the model of the same time horizon), they allowed us to better calculate the total traversal time in the optimized solutions.

By setting the values of u^m_{ijt}, we specified that each truck could carry one container, each train could carry a maximum of 54 containers, and the container capacity for each barge was 45 containers. Within a given mode, we assumed these values were constant across all arcs (i, j) and time periods t. We set the container capacity (i.e., the u_{ij}-parameters) of the road, rail, and water arcs to 300, 540, 450, respectively. This is equivalent to letting a maximum of 300 trucks, 10 trains, and 10 barges move on their respective arcs (i.e., $\bar{u}_{ij}$-parameters). The loading/unloading capacity, ϕ_i, was set to 500 containers for every intermodal node i. Because both unloading (i.e., from one transportation mode into the intermodal node) and loading (from the intermodal node into another transportation mode) count against this capacity, 250 containers can then switch from one transporting mode to another simultaneously. We set the waiting capacity on road, rail, and water nodes (i.e., μ_i-parameters) to 1, 54, 45, respectively. The inventory capacity q_i at each intermodal node i was set to 300 containers. The values mentioned in this paragraph were set to large

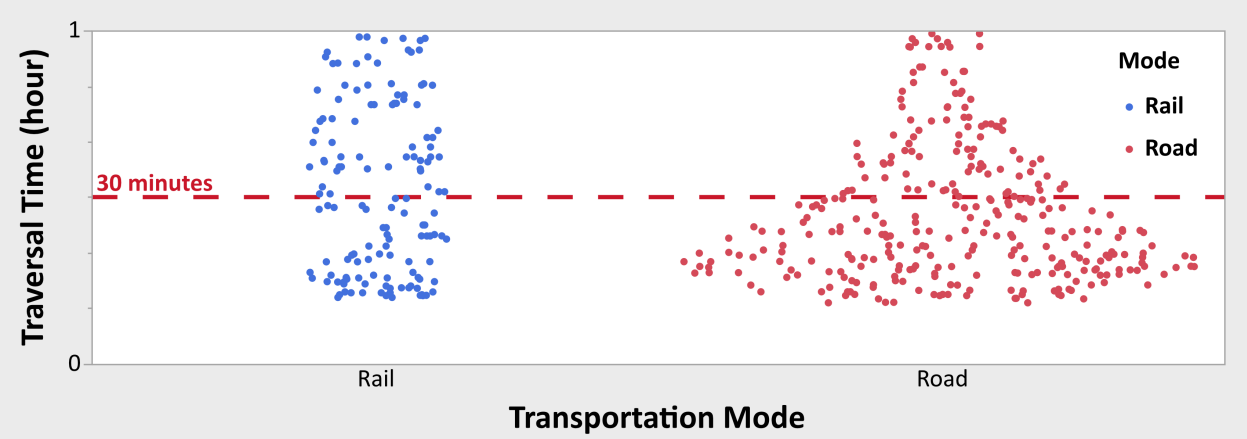

Figure 3: Scatter plot of the traversal times ($\leq$ 1 hour) for all road and rail arcs. The horizontal axis depicts the transportation mode. The vertical axis represents the traversal time in hour. Density random jitter is applied to the horizontal axis to help visualize the distribution of values.

values, so they did not become a bottleneck in the optimization problem. In addition, these values are kept consistent across all the scenarios that are described in Section 5. The values for level of functionality of arcs (i.e., λ_{ij}-parameters) are set in Section 4.4. The procedure for determining the maximum number of transporting entities in the system (i.e., ν_t^m-parameters) will be described in Section 6.1.

4.3 Model Relating Rice Yield to Fertilizer Demand Satisfaction

In our model, we seek to maximize the expected rice yield based on the amount and timing of fertilizer delivered. We proceed by explaining the impact to yield if less fertilizer is applied than necessary and/or the fertilizer application occurs later than recommended. We denote these two impacts as reduced application and late application, respectively. We assume these are not synergistic and can be applied together or separately.

For impact 1, a reduced application, we use a linear-plateau model developed previously from a series of field trials [Harrell et al., 2011]. The model predicts the yield Y (in bushels per acre, or bu/ac) as a function of the rate N of fertilizer application (in lbs Nitrogen per acre, or lbN/ac) as follows:

$$Y = \begin{cases} a + bN, & N < C \\ P, & N \geq C \end{cases} \tag{28}$$

To parameterize the model we use recent input data from Arkansas fertilization and variety trials [Castaneda-Gonzalez et al., 2020], testing eleven new rice cultivars to nitrogen fertilization rates, each in three soils (except for one that was tested in just two). We tested across every plausible value for C and optimized for the other three parameters. Across these twenty trials, the following median parameter values were found:

- $C = 121$–149 lbN/ac,

- $a = 90.3$ bu/ac,
- $b = 0.75$ $\frac{\text{bu/ac}}{\text{lbN/ac}}$,
- $P = 194$ bu/ac.

For impact 2, a late application, we fit a linear response to data on flooding timing as representative of a delay, since flood activates the fertilizer. In reality the data mixes two factors: delayed infiltration and activation of the fertilizer and loss of fertilizer via volatilization. We chose the "protected fertilizer" application that included NBPT that protects against volatilization, assuming that most of this impact is physiological in terms of the delay in getting to the plant. The data is originally from [Norman et al., 2009] and was re-summarized in the University of Arkansas rice handbook. The line of best fit can be simplified to

$$f_{\text{yield}} = -0.0077\, t_{\text{delay}}, \tag{29}$$

where f_{yield} is the fraction of the anticipated yield and t_{delay} is the number of days that the application is late.

The nitrogen fertilization rate and the application time directly affect the rice yield. We tested multiple values of C but ultimately decided to use $C = 138$ lbN/ac for our computational experiments. To determine the demand of nitrogen fertilizer at the demand nodes, we calculated the amount of fertilizer that one 40-ft container could haul. In this research, we focused on urea fertilizer as it has many advantages over other nitrogen fertilizers. Urea is safer to transport and handle, and it is less corrosive to the equipment. It has a higher analysis than other dry nitrogen fertilizers (i.e., 46-0-0); therefore, it has low transportation costs per unit of nitrogen. Lastly, it can be used on many different crops. Each container can carry 21 pallets, and each pallet can hold up to 63 of the 32-lb fertilizer bags [Milorganite, 2021]. In other words, one container can carry around 42,336 lbs of fertilizer. Because we know that urea contains 46% of nitrogen, we can estimate that one container can carry approximately 19,500 lbs of nitrogen. With $C = 138$ lbN/ac, one container can carry enough urea fertilizer to fulfill the need for 141.30 acres of rice.

The number of demand containers for each demand node was calculated by dividing the total acreage by 141.30 and rounding up to the nearest integer. For example, the demand node 90000 has 3,912 acres of land; this node requires approximately 28 containers. The total resulting demand across all demand nodes was 7,776 containers of fertilizer. The next step was to determine the amount of additional rice yield that we can expect from satisfying one container of urea fertilizer demand, assuming the fertilizer is delivered in a timely fashion. First, we calculated the additional yield that is obtained by applying urea fertilizer to an acre of rice crops. This is done by subtracting the intercept (i.e., $a = 90.3$ bu/ac) from the plateau yield (i.e., $P = 194$ bu/ac), which equals 103.7 bu/ac. Therefore, the additional rice yield per container is calculated by multiplying the additional yield per acre by the amount of fertilizer that one container can haul (i.e., 103.7 bu/ac $\times$ 141.30 ac/container $\approx 14,653$ bu/container). This value was used to determine the plateau of the yield curve, which will be discussed in further detail in the next section. Hence, in the best-case scenario where no disruption occurs and all containers are delivered in a timely manner, the optimal yield for the optimization model should be $7,776$ containers $\times\ 14,653$ bu/container $= 113,941,728$ bu.

Table 1: Summary of the number of arcs that are disrupted for each disruptions.

Disruption Scenario	Number of Disrupted Arcs
Land - Level 1	69
Land - Level 2	357
Land - Level 3	694
Water	36

4.4 Transportation Disruption Scenarios

We created disruptions scenarios for both land and water. To create the scenarios for land disruption, we gathered geographical data (i.e., Shapefile files) about the closed highways due to flooding events for 2011 and 2016–2019 from the Arkansas Department of Transportation. In order to align the obtained data with the defined network, several zones/areas with a high risk of flooding are extracted. First, a density-based spatial clustering of applications with noise (DBSCAN) algorithm is used to identify clusters that can then be used to construct the aforementioned zones. Given a set of points, DBSCAN groups together points that are close in Euclidean distance (high-density regions) and marks the outliers in the low-density regions [Ester et al., 1996]. The DBSCAN algorithm is available to use in the sklearn package in Python [Pedregosa et al., 2011]. Given each cluster of the closed road nodes of each year, a polygon can then be constructed by calculating an alpha shape (Fig. 4). The alpha shapes approach is often used for shape reconstruction from a dense unorganized set of points. A convex hull is an alpha shape when the alpha-parameter is equal to zero. The alpha-parameter can be manipulated to tighten or loosen the fit around the points, which creates a concave hull. In this research, we set the alpha parameter to 3. A Python API is used to aid in the generation of alpha shapes [Bellock, 2021]. By plotting the flooding zones of multiple years, we can see several overlapped areas where traffic is closed most frequently. The end result was the creation of three disruption levels (i.e., levels 1, 2, 3 representing the areas with low, medium, high impact due to the flooding, respectively). All arcs that intersect the zones can be assumed to be affected by the flooding zones (Table 1). Note that some demand nodes are located within these areas; thus, we can see how the disruption levels and their duration will impact the yield in the result section.

The water disruption scenario information was provided by the research team from Vanderbilt University. The data was extracted from the historical lock closure for 2015 and 2016 flooding data. The data specifies closing and reopening dates for locks in Arkansas's navigable waterway system (Fig. 5). Depending on the operational level of each lock, the incident arcs associated with the lock share the same operation level.

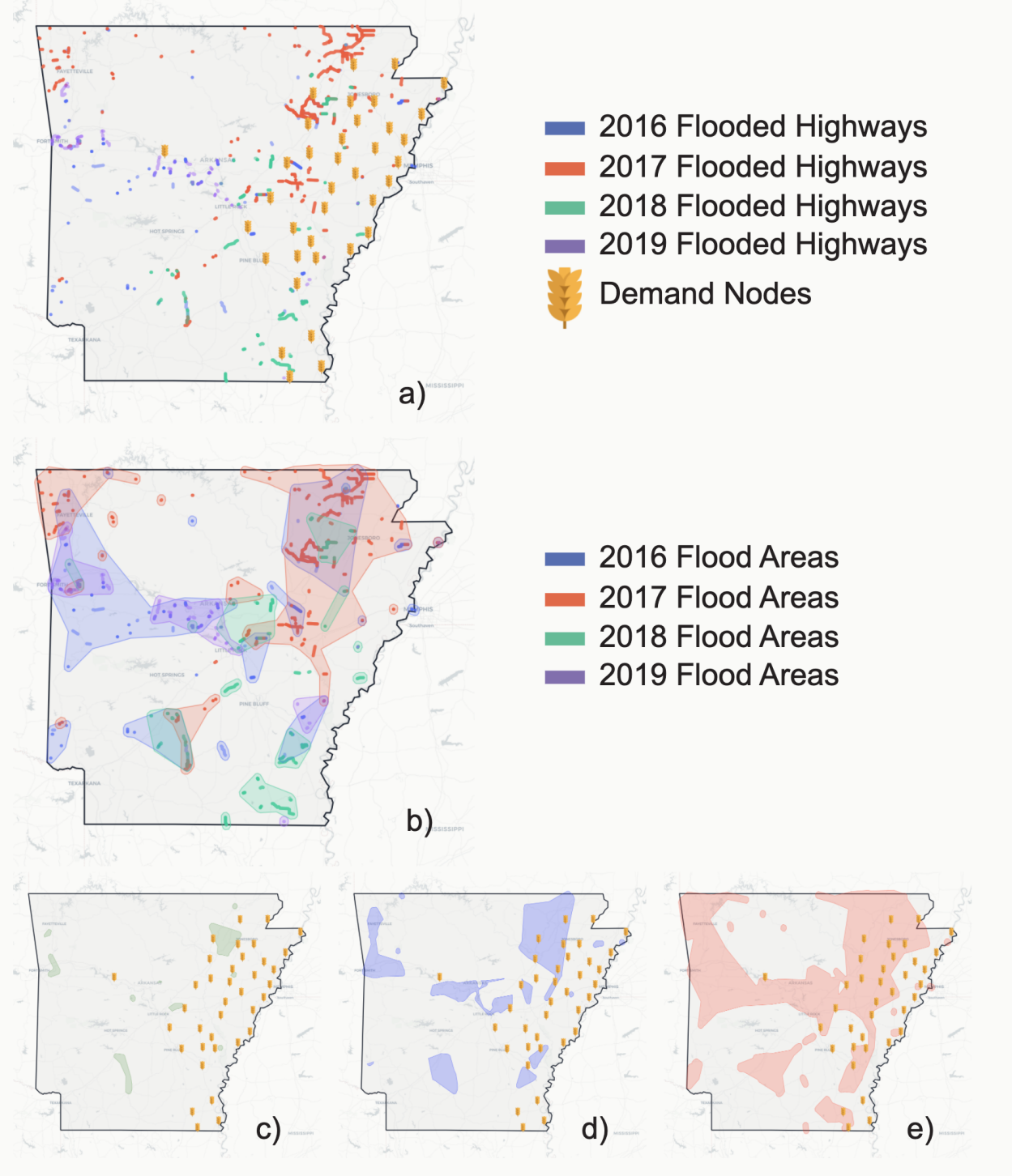

Figure 4: **a)** Closed highways in 2016-2019, **b)** alpha shapes from the DBSCAN clusters, **c)** areas with level 1 risk, **d)** areas with level 2 risk, **e)** areas with level 3 risk. Note that there are several demand nodes located inside the areas.

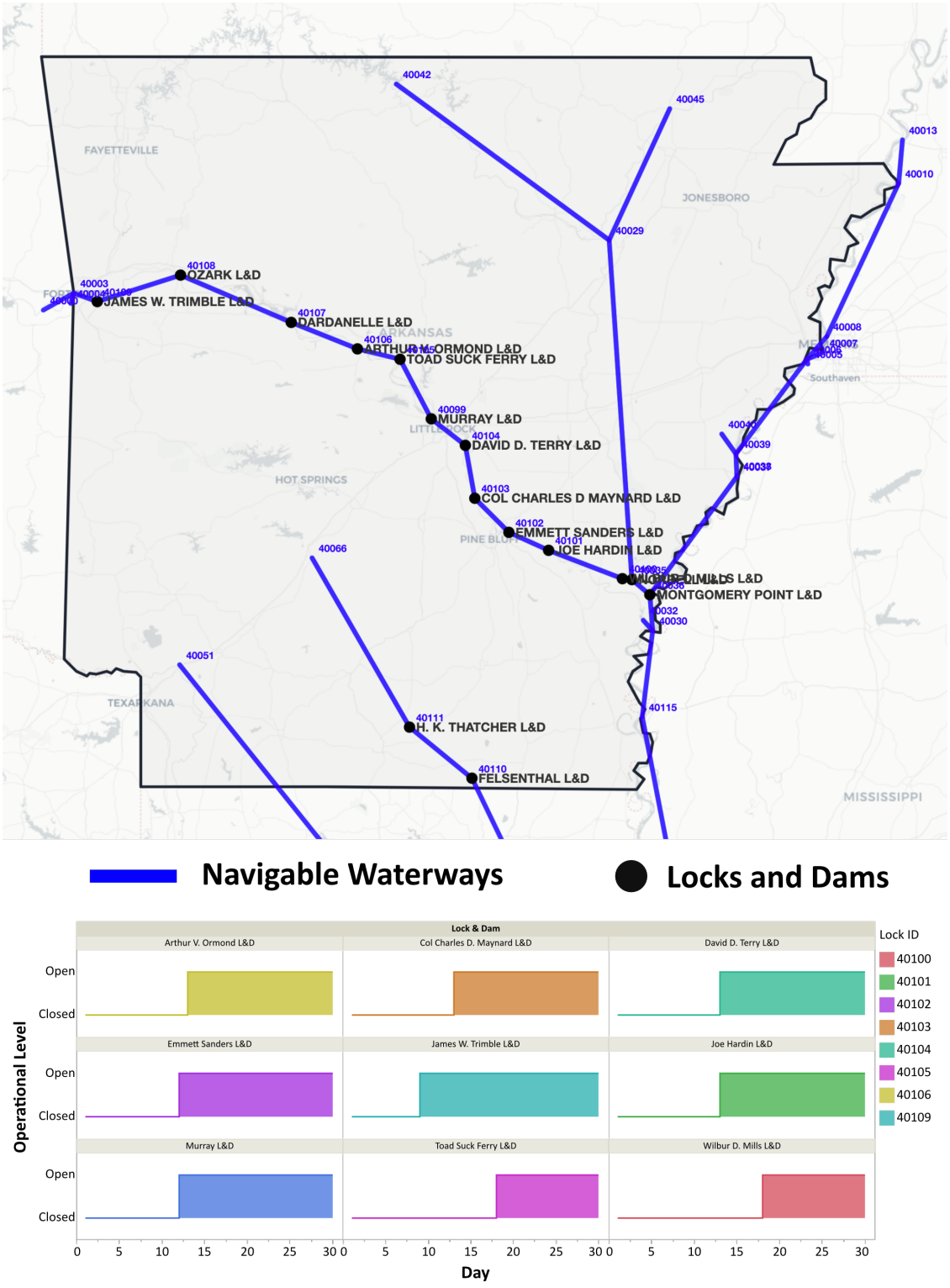

Figure 5: Location and operational level of locks and dams.

5 Experimental Setup

To evaluate the formulated optimization model performance, we developed various scenarios based on historical accounts. Our intent in the design of our experiments is to answer the following questions.

1. How does a disruption-induced reduction in the availability of transporting entities in the network impact the amount and timing of fertilizer delivery, thereby impacting yield?

2. How does the severity, start time, and duration of disruptions on the land and water transportation networks impact the ability and timeliness of satisfying fertilizer demand?

3. When given the ability to restore different numbers of disrupted transportation network arcs, which ones are selected and how does the number restored impact yield?

To answer these questions, we created scenarios over a one month time horizon (i.e., 1,440 30-minute time periods). Specifically, we examined the month from April 27 to May 26. We selected this month to coincide with the time when fertilizer is most important as we will describe in this section. Based on Hardke et al. [2021], we chose March 21 as a seeding date and May 2 as a flooding date (i.e., an average of 42 days between seeding and flooding dates provides excellent yield). The fertilizer must be applied the day before the flooding date to achieve the optimal yield. In other words, demand nodes must receive containers of urea fertilizer before May 2. As we show in Fig. 6a, the yield begins to decrease if fertilization occurs after the flooding date, as specified by Equation (29). The yield per container is 14,653 bushels of rice as long as the container is delivered before the flooding date, and it decreases linearly for each time period after the flooding date. The yield associated with each container of demand not delivered before the end of the planning horizon is assumed to be zero. Thus, our selection of April 27 as the starting date for our time horizon allows for the delivery of fertilizer 5 days prior to necessary.

To determine how changes impact our results, we first need to establish a baseline without disruptions, without the need for restoration, and with sufficient transporting entities. As follows, we first ran the model in an unconstrained environment to determine the highest possible yield. Specifically, we ran the model with a large number of transporting entities and no disruption to the transportation network to determine this best-case yield. To determine how many transporting entities are needed, we divided the total number of demanded containers by the container capacity per transporting entity (i.e., each truck, train, and barge can carry one, 54, and 45 containers, respectively). In this analysis, we assumed trucks would primarily be used for shipments with short distances (e.g., last-mile delivery); therefore, we decided to use 400 trucks instead of the 7,776 trucks that would have been needed to simultaneously carry all demanded containers. The resulting upper bounds on the number of trucks, trains, and barges were selected as 400, 150, 170, respectively. In this best-case scenario, hereafter referred to as the *baseline scenario*, we include no land or water disruptions.

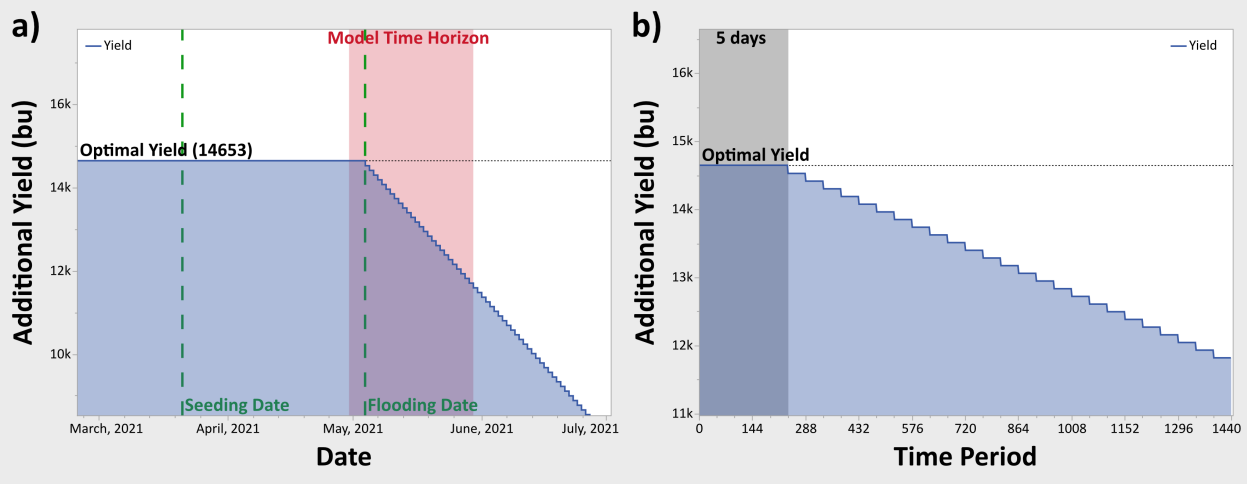

Figure 6: **a)** Additional yield per container vs. delivery date. The seeding date (March 21) and flooding date (May 2) are marked by green dashed lines. We selected the starting date of the model to be five days before the flooding date (See model time horizon in red shading). **b)** Expected yield per container vs. delivery time period over the model horizon. Each time period is 30 minutes. The time horizon of the model is one month, which is equivalent to 1440 time periods.

Fig. 7 summarizes the timing of delivered demand by demand node in the baseline scenario. The baseline scenario solution had several characteristics of note. First, all shipments were initially routed on the water arc, with a traversal time of 81 time periods; therefore, the earliest delivery time occurred in time period 85. Second, the demand nodes did not receive containers of urea all at once but instead received them in multiple shipments. For example, demand node 90004 received three shipments at times 149, 174, and 191. Because we used a conservative number of trucks, multiple trips were needed to complete the last-mile delivery to this node. For example, we used the 400 trucks in the baseline, but node 90004 requires 648 containers. Third, the model required 191 time periods (i.e., approximately four days from the beginning of the time horizon) to satisfy all demand. Thus, this gave us an insight into how to select a reasonable starting date for the optimization model. In particular, we set the starting time of the model five days (240 time periods) before the flooding date, as shown in Fig. 6b. This selection results in April 27-May 26 as the one-month time horizon and allows fertilizer delivery to occur which results in the maximum yield possible. By guaranteeing it is possible to achieve maximum yield in the baseline scenario, we can investigate the potential reduction in yield due to reduced availability of transporting entities and disruptions to the transportation network.

To answer the first question, we created additional scenarios by changing the number of transporting entities and captured the impact to the expected yield. Specifically, we varied the number of available trucks in 150, 200, 250, 300, 350, 400, the number of available barges in 30, 60, 90, 120, 150, and the number of available trains in 50, 80, 110, 140, 170. In total, we tested 150 scenarios consisting of all combinations of the number of trucks, barges, and trains. We note, for these scenarios we included neither disruptions to the transportation network nor restoration. We analyzed these results and determined that 30

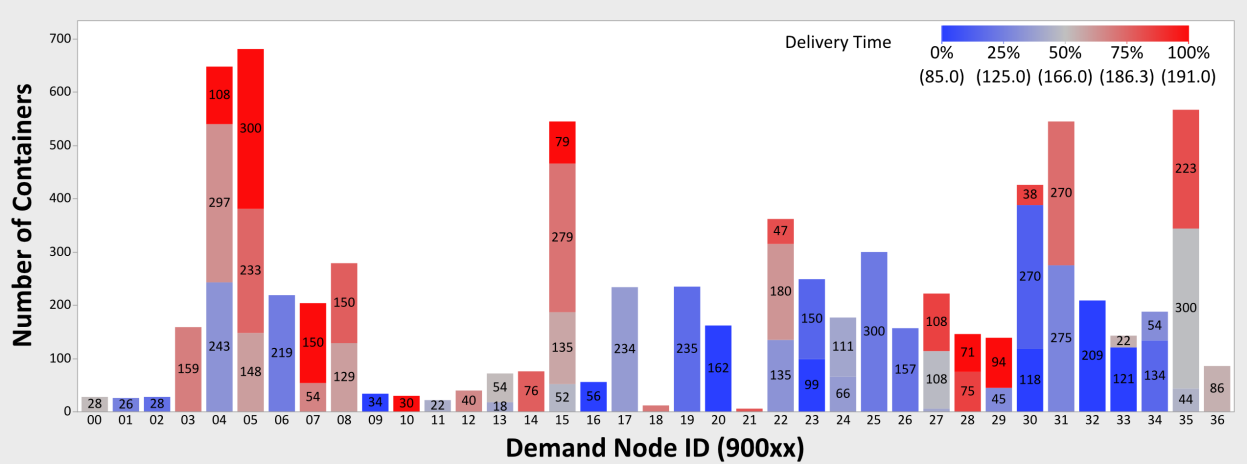

Figure 7: Number of delivered containers by demand node. The color represents the time period of delivery, which ranges between 85 and 191. Demand nodes that require a high number of containers receive the fertilizer in multiple shipments.

trains, 50 barges, and 400 trucks were sufficient to meet all fertilizer demand in the first 5 days of the time horizon (i.e., before the flooding date) and thus result in the maximum expected yield. Unless indicated otherwise, we used this level of trains, barges, and trucks for all experiments described hereafter.

Second, we investigated our next question by analyzing the impact of land and water transportation disruptions on the expected yield and amount of satisfied demand. We created 438 scenarios consisting of two equally sized subsets, one in which only land disruptions were included and one in which both land and water disruptions were included. In the first subset of scenarios, we included land transportation disruption at the three severity levels outlined in Section 4.4 with different disruption starting times and durations. Specifically, we considered land disruptions that begin in the first 14 days of the time horizon (time periods 0 to 336) and last for between 3 and 30 days. We considered all combinations of the disruption starting time in increments of 1 day (48 time periods) and disruption duration in increments of 3 days (144 time periods). We removed the combinations that had the ending time exceed the time horizon (1,440 time periods). The second subset of scenarios was identical to the first scenarios with the exception that we added disruption to the water network consistent with the explanation in Section 4.4. For the purposes of this set of experiments, we imposed that no restoration would occur by setting $B_t = 0,\ \forall t \in T$.

Lastly, we investigated our last question by allowing disrupted arcs to be restored. For this analysis, we used the scenario, which we refer to as the *worst-case* scenario, with both water disruption and land disruption starting at time 0 and lasting the entire time horizon. In this worst-case scenario, disrupted arcs can never carry flow and therefore no fertilizer can be transported to demand nodes in the disrupted area unless restoration is performed. Beginning with the worst-case scenario, we considered five restoration budgets and analyzed the optimal arcs selected to be restored and the resulting increases in yield. We assumed the entire restoration budget would be available immediately (i.e., $B_0 > 0$ and $B_t = 0,\ \forall t \in T \setminus \{0\}$). To set the budget amount B_0, we first defined the set of arcs used in the optimal solution to

the baseline case but not in the optimal solution to the worst-case scenario. Let R equal the number of arcs in this set. We note, if $B_0 \geq R$ in the worst-case scenario, it is possible to achieve the baseline yield by fully restoring all of the arcs in this set. We therefore considered smaller values of the restoration budget (specifically, $\{0.1R,\ 0.2R,\ 0.3,\ 0.4R,\ 0.5R\}$) to investigate potential for less-than-complete restoration to reduce the impact of disruptions.

The optimization model and the code for preprocessing data were developed in Python 3.7. IBM Decision Optimization CPLEX Modeling (DOcplex) package, version 12.10, was used to solve the optimization model. Results were analyzed using Python and JMP.

6 Results and Discussion

6.1 The impact of the number of available transporting entities

In this subsection, we seek to answer question 1 by quantifying how the number of available transporting entities impacts the ability and timeliness of meeting demand. As described in Section 5, we consider scenarios that vary the amount of available transporting entities relative to the baseline scenario.

Our key findings from these experiments are as follows. Our results for the scenarios in this set cause different timing of deliveries relative to the baseline scenario; however, the number of transporting entities in each scenario remains enough to satisfy all demand over our one-month time horizon. Second, the results indicate that the expected yield remains similar for most scenarios in this set; however, slight differences in yield can be observed due to the CPLEX setting, which terminates exploration of the solution space as soon as it has a solution within a specified tolerance of optimality. This effect will be discussed further in Section 6.4.

Several significant observations are as follows. First, because the water mode has the lowest penalty value, it is the most favored transportation mode as the total distance traveled by the containers greatly outweighs the others, as shown in Fig. 8a. This is in line with the intuition that shipping by water is less costly than road- or rail-based shipping, and it has high carrying capacity with fewer size and weight restrictions. We can also observe that many demand nodes are located near the navigable waterways, meaning containers can be transported by barge almost all the way to the demand node. Second, as the number of barges decreases to below 80, the model starts to utilize rail to transport the containers from the supply node to maintain the optimal yield, as shown in Fig. 8b. As a result, the total container-miles transported by rail increases 313.70%, and via barges decreases 39.63% compared to the baseline scenario. A reason for this change is that barges have the slowest transit time, meaning multiple trips could be required to meet demand; however, this may result in satisfying the demand after time period 240, causing a reduction in yield. The total container-miles transported by truck remains similar across this set of scenarios as this mode is mainly used for last-mile delivery to the demand destinations. Third, we observed a decrease in the total expected yield when the number of available barges and trains are 30 and 50 (i.e., they are the lower bound values of their respective modes). Because some containers are delivered after time period 240, the total expected yield decreases by 1,269,742 bu (1.11% of the optimal yield in the baseline scenario). The timing of delivered containers for this

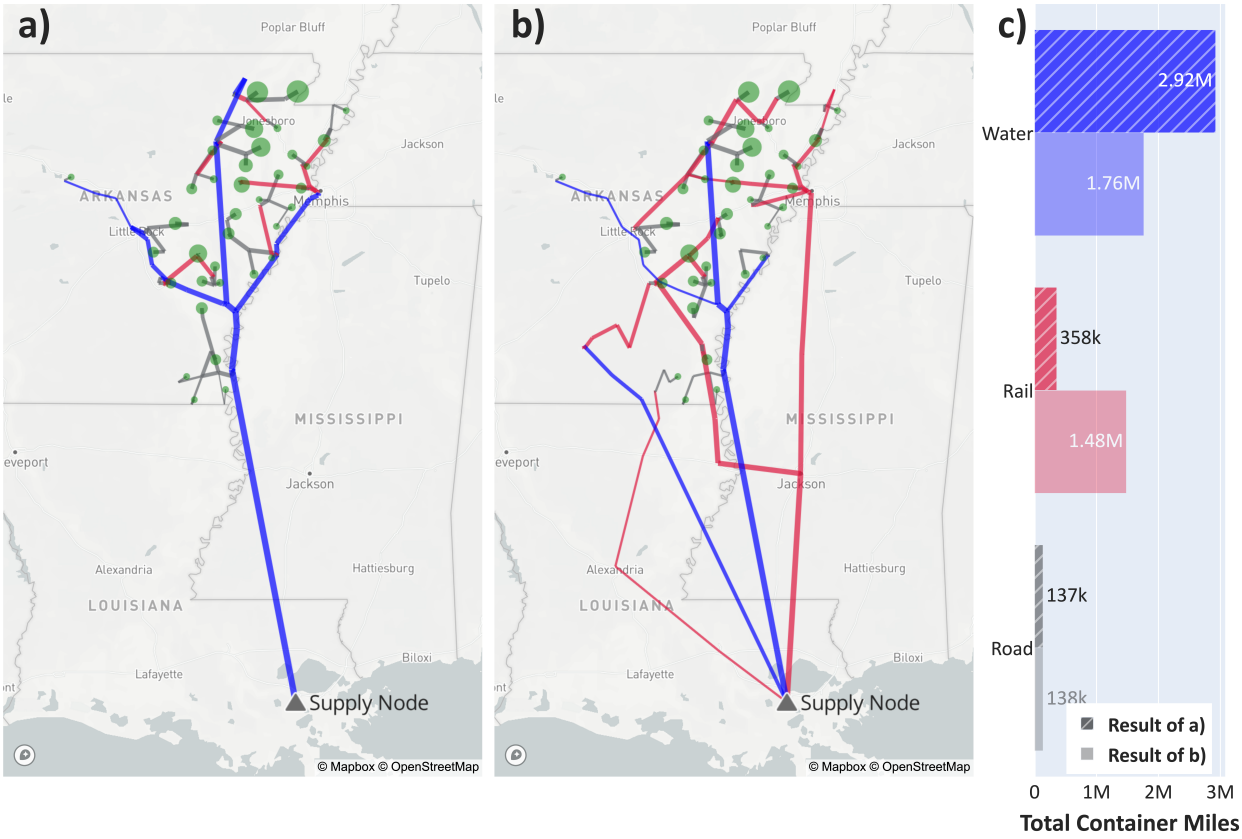

Figure 8: **a)** Model solution when the number of barges is greater than 80, **b)** Model solution when the number of barges is less than or equal to 80, **c)** Total container miles for different transporting modes.

scenario is shown in Table 2. Based on our observations, more than 30 trains and more than 50 barges is sufficient to achieve the baseline yield (Fig. 9). However, yield does not appear to be sensitive to the number of trucks between 150 and 400.

We used regression to understand the relationship between the response (i.e., total expected yield) and the predictor variables (i.e., the number of trucks, the number of trains, the number of barges, and all two-way interactions). The p-value for each predictor tests the null hypothesis that its coefficient is equal to zero (i.e., the predictor has no effect). A p-value that is less than 0.05 indicates that the changes in the predictor's value are related to the changes in the total expected yield. Conversely, a large p-value suggests that the predictor's changes are not related to the changes in the response. Table 3 shows the list of model effects, sorted by increasing p-values. There is an interaction between the number of barges and the number of trains on the total expected yield. This means that the effect of the barges changes as we change the number of trains. As we indicated previously, the number of trucks is not statistically significant, meaning that the number of trucks used will not affect the optimum yield.

Table 2: The timing of deliveries when the numbers of barges and trains are 30 and 50, respectively.

Baseline total yield: 113,941,728 **Total yield in this scenario**: 112,671,986			
Delivery Time Interval	**Number of Delivered Containers**	**Yield Per Container**	**Total Yield**
$[56 - 239]$	4,915	14,653	72,019,495
$[336 - 383]$	1,125	14,407	16,207,875
$[432 - 479]$	1,736	14,081	24,444,616

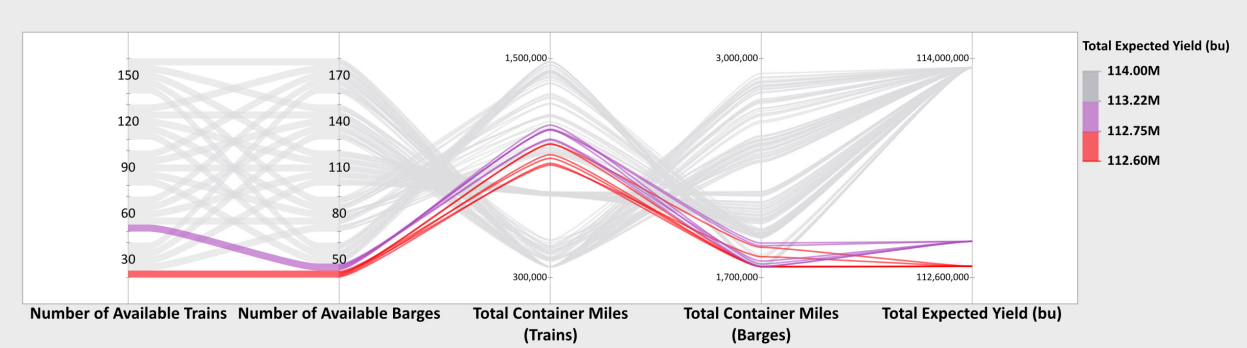

Figure 9: Parallel coordinates plot comparing the number of transporting entities, their total container miles, and the total expected yield. Each series (i.e., a line that begins on the left side of the plot and ends on the right side of the plot) corresponds to a scenario of the optimization model, where the scenario's number of available trains, number of available barges, total container-miles by train, total container-miles by barge, and total expected yield are each plotted in one of the five vertical bars. The total container-miles for trucks was omitted from the plot because it is similar across all scenarios.

Table 3: Effect summary sorted by the ascending p-values. The effect that has p-value values less than 0.05 indicate that it is statistically significant.

Effects	p**-value**
# of barges	0.00037
# of trains * # of barges	0.02777
# of trucks * # of trains	0.09173
# of trains	0.30142
# of trucks * # of barges	0.42677
# of trucks	0.80433

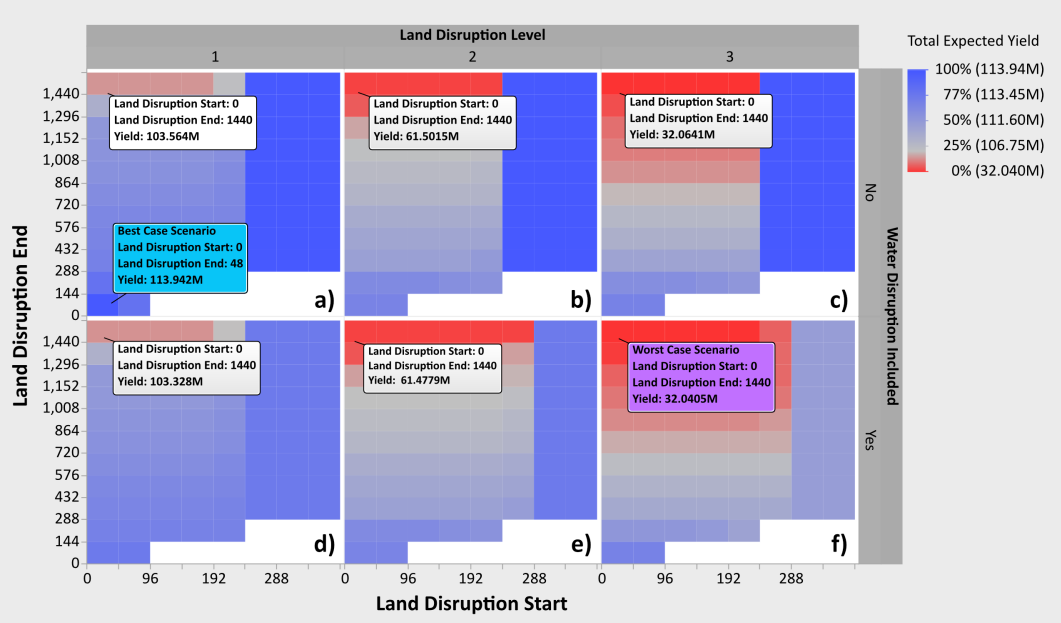

Figure 10: Heat map of the total expected yield. The horizontal axis represents the land disruption starting time and the vertical axis represents the land disruption ending time. Results for 3 different land disruption levels with no water disruption are displayed in subplots **a-c** and results with water disruption are displayed in subplots **d-f**. The white label in each plot displays the total expected yield in the scenario where the disruption happens for the entire time horizon. The label for the worst case scenario (i.e., subplot **f**) is colored purple which shows the smallest expected yield.

6.2 The impact of disruption

In this section, we present the results of our investigation on how disruptions to the land and water transportation networks impact the timing and ability to meet fertilizer demand. Before going into further detail, we should note that several demand nodes are located inside the disruption zones. Therefore, if the disruption happens for the entire time horizon, these demand nodes will not receive the containers of fertilizer which significantly reduces the total expected yield.

In Fig. 10, we illustrated the relationship between the length, starting time, and level of disruption with respect to the expected yield. From this figure, we observe that the yield is greatly impacted by disruptions that occur early in the time horizon and last for longer periods of time. Further, we note that water disruption has a greater impact later when coupled with land disruptions that occur later in the time horizon. Lastly, we observe that high-level disruptions and long-duration disruptions have the greatest impact on yield. For the higher-level disruptions, the duration does not need to be as long as lower-level disruptions to see the great impact to yield. As mentioned earlier, all demands are satisfied within the first 240 time periods in the baseline scenario. Therefore, when there is no water disruption and the land disruption starts after time 288, the total expected yield is achieved and the length of the disruption does not matter.

In Table 4, we summarize the characteristics of the three land transportation disruption

Table 4: The characteristics of each disruption level.

Land Disruption Level	**Number of Affected Demand Nodes**	**Total Affected Demand (containers)**	**Worst-Case Reduction in Yield (bushels)**
1	2	691	10,125,223
2	11	3,526	51,666,478
3	22	5,544	81,236,232

Table 5: Disruption effect summary sorted by ascending p-values (where insignificant effects, with $p > 0.05$, are excluded).

Effects	p**-value**
Land disruption duration	0.00000
Land disruption level	0.00000
Land disruption level * Land disruption duration	0.00000
Land disruption start * Land disruption duration	0.00005
Water disruption included	0.00088
Land disruption start	0.00164
Land disruption level * Water disruption included	0.00184
Water disruption included * Land disruption duration	0.01041

levels, the number of affected demand nodes, the total demand impacted, and the worst-case impact to yield. To interpret this table, if a level-3 disruption occurs for the entire one-month time horizon, then 22 out of the 37 demand nodes will not have any of their fertilizer demand met which will result in a reduction to yield from 113.942 million to 32.064 million bushels of rice for the state of Arkansas.

We also conducted a regression analysis to study the relationship between the total expected yield and various disruption's effects. In Table 5, we present the effects in this analysis including the starting time, duration/ending time, level of land disruption, whether or not the water disruption was included, and their two-way interactions. We note that all effects have p-values below 0.05 and land disruption level and duration are particularly significant. This is consistent with our finds shown in Fig. 10. Another observation is that the addition of water disruption also has a negative impact on the total yield.

Finally, by comparing our model's solutions for the baseline and worst-case scenarios, we examined the impact of disruption on the resulting transportation routes and modes used to satisfy demand. Figs. 11a and 11b respectively illustrate the flow of the containers in the baseline and worst-case scenarios. In the worst-case scenario, only 15 demand nodes (corresponding to 28.7% of the total demand) met their fertilizer requirement. In both the

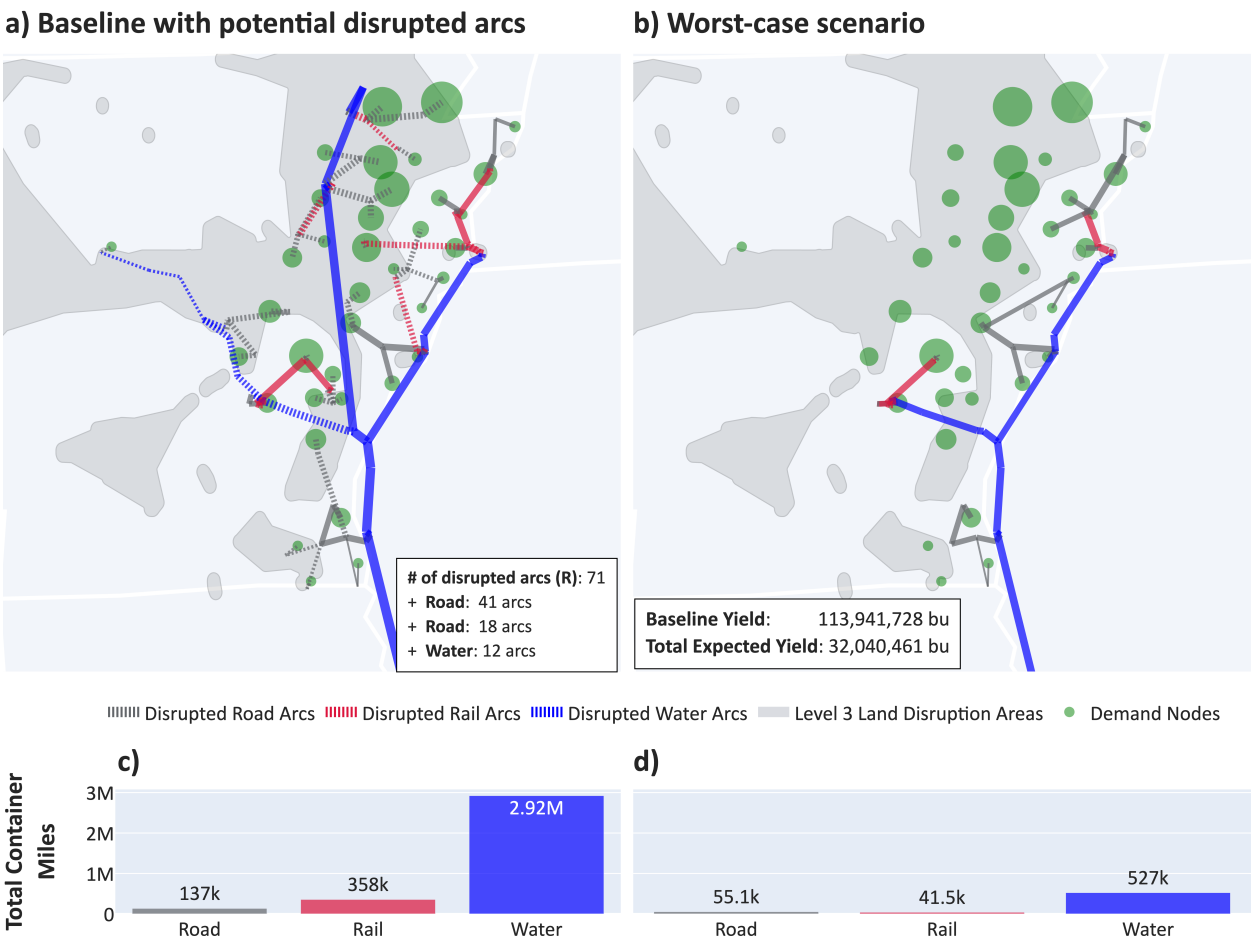

Figure 11: **a)** Illustration of commodity flows in the baseline scenario, where a dashed line indicates the arc is disrupted in the worst-case scenario. **b)** Illustration of commodity flows in the worst-case scenario (i.e., with water disruption and level 3 land disruption). Illustrations of total container-miles by three transportation modes in the baseline (i.e., subplot **c**), and in the worst-case scenario (i.e., subplot **d**). The nodes and arcs are sized according to the total fertilizer demands and the commodity flows.

baseline and worst-case scenarios, water was the primary mode to transport the fertilizer; however, the total container-miles of all transporting modes are significantly decreased due to the disruption (Fig. 11d).

6.3 The impact of restoration

In this section, we present the results of our investigation into the impact of the ability to restore a subset of the disrupted arcs. As previously mentioned, there were $R = 71$ arcs — 41 road arcs, 18 rail arcs, and 12 water arcs — used in the optimal solution to the baseline scenario and all were disrupted in the worst-case scenario. We solved five scenarios in which we varied the first time period's restoration budget B_0 in $\{0.1R, 0.2R, 0.3R, 0.4R, 0.5R\}$ thereby

representing that we can restore between 10% and 50% of the 71 arcs used in the optimal solution to the baseline scenario. We set $B_t = 0$, $\forall t \neq 0$.

In Fig. 12, we illustrate the arcs disrupted, restored, and used under the five different restoration budget levels. The budget level impacts our ability to achieve the highest possible yield. When we are able to restore 40% and 50% of the arcs used in the baseline scenario, we are able to achieve the maximum yield. However, the yield decreases by 15.668, 5.474, and 3.485 million bushels of rice for budgets equal to $0.1R$, $0.2R$, and $0.3R$ respectively. All demand was met for all restoration levels, however the lower restoration budgets caused demand to occur after the flooding date which impacts yield. In other words, we did not have sufficient budget for restoring the arcs so they could have enough capacity for the containers to flow through.

We consider continuous, non-binary restoration of arcs. Thus, if an arc is selected to be restored, it is most commonly not restored to full operation. For example, demand node 90001 is located inside the disruption zone, and arc (220, 90001) is the road arc that connects the road network to this demand node, the solution indicates that this arc was restored only 1.67% at time 0 (i.e., $D_{220,90001,0} = 0.01667$). As a result of this partial restoration, five containers per time period were able to be transported on this arc. This can be verified by looking at the timing of the deliveries at this node. In particular, this demand node required 26 fertilizer containers; it received six different shipments as follows: five shipments of 5 containers were delivered at times 159, 177, 181, 221, 235, and a shipment of 1 container was delivered at time 23. Despite the disruptions in these scenarios, the latest delivery time was still under 240 and the same number of containers, albeit in multiple shipments, were delivered. In the baseline scenario, this node received 26 containers in a single shipment.

In scenarios with budgets of $0.4R = 28.4$ and $0.5R = 35.5$, the model prioritizes its budget toward restoring road arcs associated with demand nodes that require a higher number of fertilizer containers. For example, demand node 90035 requires 567 containers. Thus, the cumulative restoration for the arc (4908, 90035) was relatively high at 96.67

By observing the aggregate flow of the containers and the total container-miles by transport modes for each scenario, we noticed several findings. First, water remained the most favored transport mode. As previously mentioned, barges could carry containers almost all the way to the demand nodes (Fig. 12c, f, and i). Furthermore, most of the barge traffic was on the White and Mississippi Rivers, where no water disruption occurred. Second, when the restoration budget was set to $0.1R$, no damaged rail arcs were restored. The model preferred to spend the limited budget on restoring the road arcs that connect the water network to the demand nodes. The reason could be that reducing the types of transportation used also reduces the number of arcs which need to be restored. As shown in Fig. 12a, no rail arcs were used in the disrupted zones. As a result, the total container-miles transported by trains is significantly lower than in the baseline scenario. Third, although three scenarios did not achieve the baseline's expected yield, we can observe some patterns in the routes. For example, the four southern demand nodes (i.e., 90000, 90001, 90020, and 90021) received the containers that were transferring from barges to trucks at the same intermodal node. Finally, as more budget was available, the containers' flow became similar to the baseline (Fig. 12c) as disrupted arcs were restored.

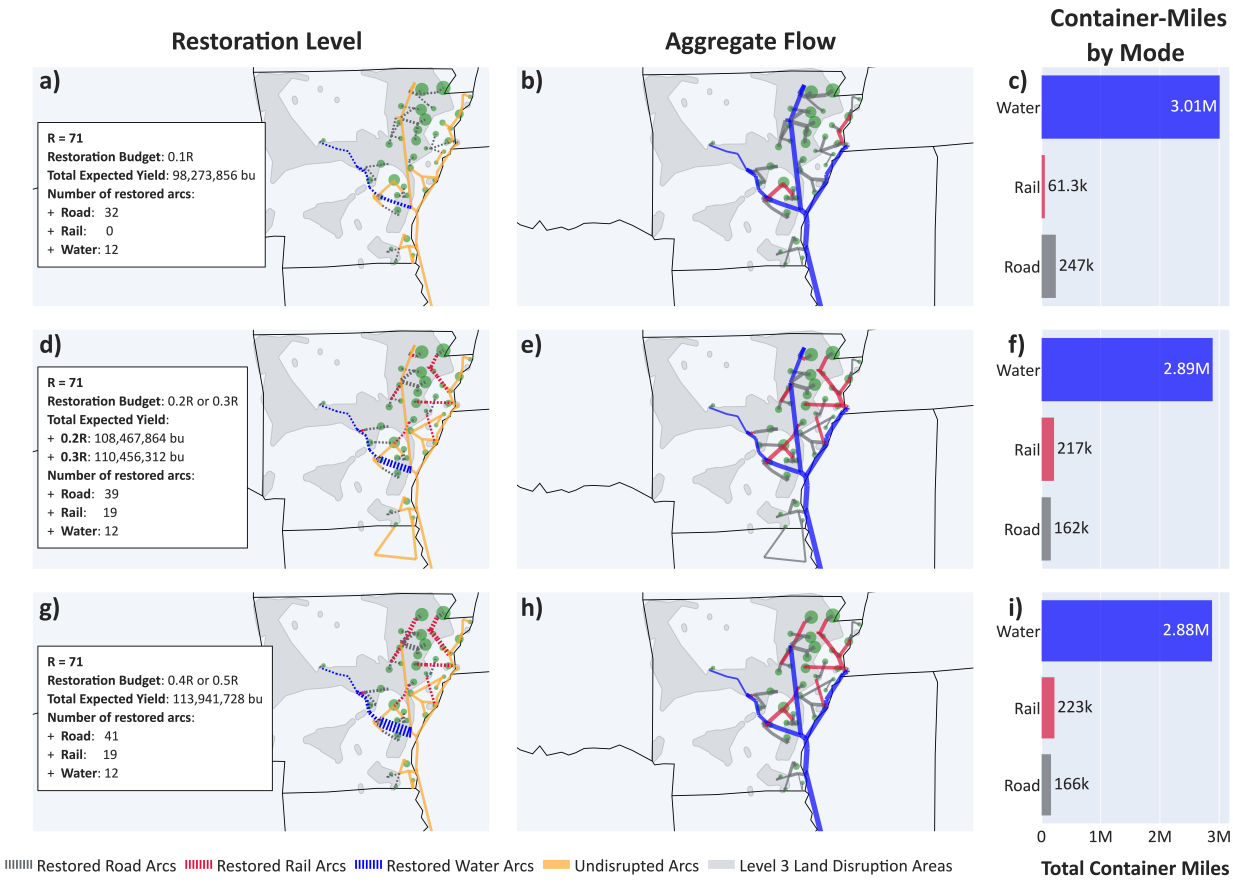

Figure 12: Illustration of the restoration plan when the restoration budget was $0.1R$ (i.e., subplot **a**), $0.2R$ or $0.3R$ (i.e., subplot **d**); and $0.4R$ or $0.5R$ (i.e., subplot **g**). Illustrations for the scenarios with a budget of $0.2R$ and $0.3R$ are grouped together because they share similar restoration plans except for slight changes in the restoration level. The same goes for the last two scenarios that included restoration. In subplots **(a, d**, and **g)**, restored arcs are indicated by dashed arcs and each arc's restoration level is indicated by its thickness. The resulting commodity flows are shown in subplots **(b, e**, and **f)** for the three restoration plan groups, respectively. Illustration of container-miles transported by mode (i.e., subplots **c, f**, and **i**) for the groups mentioned above.

6.4 Computational challenges with time

This section discusses the computational challenge of solving the formulated optimization model and two approaches to overcome this challenge. Because the model consists of millions of variables and constraints, CPLEX sometimes requires significant time to find an optimal solution. In general, CPLEX can find a feasible solution within the first two hours of solve time. Therefore, we limited the elapsed time spent solving the model to six hours. Second, we instructed CPLEX to stop as soon as it has found a feasible solution proved to be within 0.1 percent of optimal (i.e., the MIP gap tolerance is set to 0.001). CPLEX terminates optimization and reports the current best possible result if it meets either stopping criteria.

In some cases, during the optimization process, the branch-and-bound tree becomes so large and exceeds the machine's available memory, which causes CPLEX to crash. For this reason, we utilized a high-memory partition (i.e., himem72) in the Arkansas High Performance Computing Center [AHPCC], which has more than 192 GB of shared memory for each node. This partition allows jobs to run for the maximum runtime of 72 hours. To utilize this resource, we divided the scenarios into six batches. These batches were concurrently running. A master Python script for each batch was created to automatically run the next optimization model once the previous one finished. Note that the computational time for scenarios with a low number of transporting entities is significantly higher than the others. More specially, eight scenarios hit the wall time of six hours. The computational time for the baseline, scenarios with disruption and 5 scenarios with restoration budget is around 161.34 minutes on average.

7 Impacts/Benefits of Implementation

In this project we built a data-driven model that is a simplified, but tractable, representation of transportation disruptions and their subsequent impact on the agriculture sector. This model provides a baseline for more advanced disruption and ongoing logistics modeling, scenario building, and can guide stakeholder discussions.

The results demonstrate the potential impact of coordination between different state and federal transportation entities (e.g., state DOTs, U.S. Army Corps of Engineers). Specifically, we demonstrate that even small amounts of coordinated restoration of damaged transportation waterways and roads causes significant benefits for agricultural yield. The research demonstrates the need for coordination, systems thinking, and understanding of how transportation impacts other interdependent infrastructures.

This model helps establish a methodology for planning in the agricultural sector. For example, it could help build guidelines for the storage size of fertilizer or seed inventory containers to provide sufficient material to withstand likely (or extreme) disruptions to the transportation sector. It could help farmers and their financial backers to plan for economic impacts of these disruptions; this financial impact could also be used to generate support for public investment in redundant or more resilient transportation infrastructure.

8 Recommendations and Conclusions

Using our model, we investigated the potential for disruptions to the multimodal transportation network to result in delayed delivery of fertilizer to rice farms in Arkansas, thereby causing reduced harvest yields. Empirically, our results suggest that the impact to rice yields is small except in the case of severe disruption (e.g., a level-3 land disruption for 2 weeks or level-2 land disruption for 3 weeks). Additionally, our results demonstrate potential for these impacts to be reduced by selectively repairing damaged portions of the transportation infrastructure immediately following the disruption or by improving the transportation system (e.g., through redundancy or storage) to limit the potential for disruption.

Our model and analysis have several limitations that may prompt future research. Although we model FA's dependendence on one important commodity, there are many other interdependencies related to FA that we have not modeled. Additionally, our model neglects that other industries and/or sectors may similarly depend on the transportation network, thus creating additional congestion and competition for resources in the event of a disruption. Follow-on research may therefore seek to model additional FA interdependencies or interdependencies with other infrastructures.

Despite the study's limitations highlighted above, the following findings provide a promising pathway for modeling and quantifying the interdependence between transportation and agriculture systems. Our study leads to the recommendation for seamless coordination between state and federal transportation organizations and different FA sectors to best understand how disruptions, rerouting, and restoration actions impact overall transportation functionality. This functionality is what enables other critical infrastructure systems, such as agriculture to best operate.

References

AHPCC. Arkansas HPCC User Support Wiki - Equipment/Selecting Resources. `https://hpcwiki.uark.edu/doku.php?id=equipment`. [Online, accessed on 04/13/2021].

O. Ahumada and J. R. Villalobos. Application of planning models in the agri-food supply chain: A review. *European Journal of Operational Research*, 196(1):1–20, 2009. ISSN 0377-2217. doi: https://doi.org/10.1016/j.ejor.2008.02.014.

J. Azucena, B. Alkhaleel, H. Liao, and H. Nachtmann. Hybrid simulation to support interdependence modeling of a multimodal transportation network. *Simulation Modelling Practice and Theory*, 107:102237, 2021.

K. Bellock. Python package index - alpha shape toolbox, 2021. URL `https://pypi.org/project/alphashape/`.

W. Burgholzer, G. Bauer, M. Posset, and W. Jammernegg. Analysing the impact of disruptions in intermodal transport networks: A micro simulation-based model. *Decision Support Systems*, 54(4):1580–1586, 2013.

S. R. Carroll, K. N. Le, B. Moreno-García, and B. R. K. Runkle. Simulating soybean–rice rotation and irrigation strategies in arkansas, usa using apex. *Sustainability*, 12(17), 2020. ISSN 2071-1050. doi: 10.3390/su12176822.

Castaneda-Gonzalez, E., Roberts, T.L., Hardke, J.T., Slaton, N.A., Moldenhauer, K.A.K., Sha, X., Frizzell, D.L., Duren, M.W., Frizzell, T.D. Grain yield response of eleven new rice cultivars to nitrogen fertilization. Technical report, University of Arkansas System Division of Agriculture, 2020. URL `https://aaes.uark.edu/communications/publications/`.

L. Chen and E. Miller-Hooks. Resilience: an indicator of recovery capability in intermodal freight transport. *Transportation Science*, 46(1):109–123, 2012.

P. D'Odorico, K. F. Davis, L. Rosa, J. A. Carr, D. Chiarelli, J. Dell'Angelo, J. Gephart, G. K. MacDonald, D. A. Seekell, S. Suweis, et al. The global food-energy-water nexus. *Reviews of Geophysics*, 56(3):456–531, 2018.

J. Doerpinghaus, S. Nurre Pinkley, K. M. Sullivan, and B. R. K. Runkle. Classifying interdependencies in the food and agriculture critical infrastructure sector. Technical report, Industrial Engineering, University of Arkansas, 2021.

N. Enayaty Ahangar, K. M. Sullivan, and S. G. Nurre. Modeling interdependencies in infrastructure systems using multi-layered network flows. *Computers Operations Research*, 117:104883, 2020. ISSN 0305-0548. doi: https://doi.org/10.1016/j.cor.2019.104883.

L. English, J. Popp, and W. Miller. Economic contribution of agriculture and food to arkansas' gross domestic product 1997-2019. *Research Reports and Research Bulletins*, Nov. 2020. URL `https://scholarworks.uark.edu/aaesrb/47`.

M. Ester, H.-P. Kriegel, J. Sander, and X. Xu. A density-based algorithm for discovering clusters in large spatial databases with noise. In *Proceedings of the Second International Conference on Knowledge Discovery and Data Mining*, KDD'96, pages 226–231, Portland, Oregon, Aug. 1996. AAAI Press.

R. S. Gray. Agriculture, transportation, and the covid-19 crisis. *Canadian Journal of Agricultural Economics/Revue canadienne d'agroeconomie*, 68(2):239–243, 2020. doi: https://doi.org/10.1111/cjag.12235.

Ç. U. Güler, A. W. Johnson, and M. Cooper. Case study: energy industry economic impacts from ohio river transportation disruption. *The Engineering Economist*, 57(2):77–100, 2012.

Y. Y. Haimes and P. Jiang. Leontief-based model of risk in complex interconnected infrastructures. *Journal of Infrastructure Systems*, 7(1):1–12, 2001.

Y. Y. Haimes, B. M. Horowitz, J. H. Lambert, J. R. Santos, C. Lian, and K. G. Crowther. Inoperability input-output model for interdependent infrastructure sectors. I: Theory and methodology. *Journal of Infrastructure Systems*, 11(2):67–79, 2005.

J. Hardke, Y. Wamishe, G. Lorenz, and N. Bateman. Rice production handbook. Technical report, University of Arkansas Division of Agriculture Cooperative Extension Service, 2021. URL `https://www.uaex.edu/publications/pdf/mp192/mp192.pdf`.

D. L. Harrell, B. S. Tubaña, J. Lofton, and Y. Kanke. Rice response to nitrogen fertilization under stale seedbed and conventional tillage systems. *Agronomy Journal*, 103(2):494–500, 2011. doi: https://doi.org/10.2134/agronj2010.0376.

E. O. Heady and J. A. Schnittker. Application of input-output models to agriculture. *Journal of Farm Economics*, 39(3):745–758, 1957.

M. Hightower. Consumers likely to feel impacts of I-40 bridge closure, 2021. URL `https://www.uaex.uada.edu/media-resources/news/2021/may2021/05-20-2021-Ark-I-40-Bridge-Ag.aspx`.

M. Huang, X. Hu, and L. Zhang. A decision method for disruption management problems in intermodal freight transport. In *Intelligent Decision Technologies*, pages 13–21. Springer, 2011.

M. Jarke, T. X. Bui, and J. M. Carroll. Scenario management: An interdisciplinary approach. *Requir. Eng.*, 3(3/4):155–173, 1998. doi: 10.1007/s007660050002.

O. Karkacier and Z. G. Goktolga. Input–output analysis of energy use in agriculture. *Energy Conversion and Management*, 46(9-10):1513–1521, 2005.

J. D. Kinsey. The new food economy: Consumers, farms, pharms, and science. *American Journal of Agricultural Economics*, 83(5):1113–1130, 2001. doi: https://doi.org/10.1111/0002-9092.00259.

W. Leontief. *Input-Output Economics*. Oxford University Press, 1966.

W. W. Leontief. Input-output economics. *Scientific American*, 185(4):15–21, 1951.

MARAD. The Impacts of Unscheduled Lock Outages Study, 2017. URL `https://www.maritime.dot.gov/ports/impacts-unscheduled%C2%A0lock-outages-study`. [Online; accessed 06-21-2021].

D. Mendonça and W. A. Wallace. Impacts of the 2001 World Trade Center attack on New York City critical infrastructures. *Journal of Infrastructure Systems*, 12(4):260–270, 2006.

E. Miller-Hooks, X. Zhang, and R. Faturechi. Measuring and maximizing resilience of freight transportation networks. *Computers & Operations Research*, 39(7):1633–1643, 2012.

Milorganite. Milorganite retailer specifications, 2021. URL `https://www.milorganite.com/retailers/product-information/product-specifications`. [Online; Accessed on 04/26/2021].

K. S. Nelson, M. D. Abkowitz, and J. V. Camp. A method for creating high resolution maps of social vulnerability in the context of environmental hazards. *Applied Geography*, 63:89–100, 2015. ISSN 0143-6228.

R. J. Norman, C. E. Wilson, N. A. Slaton, B. R. Griggs, J. T. Bushong, and E. E. Gbur. Nitrogen fertilizer sources and timing before flooding dry-seeded, delayed-flood rice. *Soil Science Society of America Journal*, 73(6):2184–2190, 2009. doi: https://doi.org/10.2136/sssaj2008.0309.

S. G. Nurre, B. Cavdaroglu, J. E. Mitchell, T. C. Sharkey, and W. A. Wallace. Restoring infrastructure systems: An integrated network design and scheduling (INDS) problem. *European Journal of Operational Research*, 223(3):794–806, 2012. ISSN 0377-2217.

M. Ouyang. Review on modeling and simulation of interdependent critical infrastructure systems. *Reliability engineering & System Safety*, 121:43–60, 2014.

F. Oztanriseven and H. Nachtmann. Economic impact analysis of inland waterway disruption response. *The Engineering Economist*, 62(1):73–89, 2017.

F. Pedregosa, G. Varoquaux, A. Gramfort, V. Michel, B. Thirion, O. Grisel, M. Blondel, P. Prettenhofer, R. Weiss, V. Dubourg, J. Vanderplas, A. Passos, D. Cournapeau, M. Brucher, M. Perrot, and E. Duchesnay. Scikit-learn: Machine learning in Python. *Journal of Machine Learning Research*, 12:2825–2830, 2011.

S. M. Rinaldi, J. P. Peerenboom, and T. K. Kelly. Identifying, understanding, and analyzing critical infrastructure interdependencies. *IEEE Control Systems Magazine*, 21(6):11–25, 2001.

J. A. Schnittker. Application of input-output analysis to a regional model stressing agriculture. 1956.

C. A. Scott, M. Kurian, and J. L. Wescoat. The water-energy-food nexus: Enhancing adaptive capacity to complex global challenges. In *Governing the Nexus*, pages 15–38. Springer, 2015.

M. Smith, J. Healy, and T. Williams. 'It's Probably Over for Us': Record Flooding Pummels Midwest When Farmers Can Least Afford It. *The New York Times*, Mar. 2019. ISSN 0362-4331. URL https://www.nytimes.com/2019/03/18/us/nebraska-floods.html.

M. SteadieSeifi, N. P. Dellaert, W. Nuijten, T. Van Woensel, and R. Raoufi. Multimodal freight transportation planning: A literature review. *European Journal of Operational Research*, 233(1):1–15, 2014.

The Fertilizer Institute. U.S. fertilizer production and mining facility at a glance. Technical report, The Fertilizer Institute, 2021. URL https://www.tfi.org/sites/default/files/images/usproductionmaps%28updated-\%29.pdf. [Online; accessed 04-15-2021].

U.S. Census Bureau. TIGER/Line Shapefiles. URL https://www.census.gov/geographies/mapping-files/time-series/geo/tigerline-file.2019.html. [Online; accessed 02-19-2021].

USDA-NASS. Quickstats. URL https://quickstats.nass.usda.gov/results. [Online; Accessed on 06/27/2021].

S. S. Wiener, N. L. Álvarez Berríos, and A. B. Lindsey. Opportunities and challenges for hurricane resilience on agricultural and forest land in the U.S. Southeast and Caribbean. *Sustainability*, 12(4), 2020. doi: 10.3390/su12041364.

R. Zimmerman, Q. Zhu, and C. Dimitri. Promoting resilience for food, energy, and water interdependencies. *Journal of Environmental Studies and Sciences*, 6(1):50–61, 2016.